

Melting transitions in aluminum clusters: The role of partially melted intermediates

Colleen M. Neal, Anne K. Starace, and Martin F. Jarrold

Chemistry Department, Indiana University, 800 East Kirkwood Avenue, Bloomington, Indiana 47405, USA

(Received 19 May 2007; published 14 August 2007)

Heat capacities have been measured as a function of temperature for aluminum cluster cations with 16–48 atoms. Some clusters show peaks in their heat capacities that are attributed to melting transitions. The smallest cluster to show a well-defined melting transition is Al_{28}^+ . For clusters with significant peaks in their heat capacities, the results can be fitted by a two-state model incorporating only solidlike and liquidlike clusters. This indicates that these clusters melt directly, that is, without the involvement of partially melted intermediates. Our previously reported heat capacity measurements for clusters with 49–83 atoms have been reanalyzed using the two-state model and a three-state model that incorporates an intermediate state. Most of the melting transitions can be fitted using the two-state model. However, for a few clusters, the heat capacity peaks are either too broad or possess shoulders, and the three-state model is required to fit the experimental results. Both premelting and “postmelting” behaviors (where the second peak is smaller than the first) are observed. Using the models, we have determined melting temperatures and latent heats for clusters with 25–83 atoms. The melting temperatures and latent heats show large (and uncorrelated) size-dependent fluctuations. While most clusters have depressed melting temperatures, there are three regions of high melting temperatures (around 37, 47, and 66 atoms) where the melting temperatures approach or exceed the bulk melting point.

DOI: 10.1103/PhysRevB.76.054113

PACS number(s): 36.40.Ei, 61.46.Bc

INTRODUCTION

When dimensions shrink into the nanometer size regime, properties that are intensive in the macroscopic world become size dependent. Phase transitions are one example: below about 10^6 atoms, the melting points of small particles begin to shift to significantly lower temperatures.^{1–4} This decrease results from the increase in the surface to volume ratio and was first predicted by Pawlow in 1909.⁵ Since phase transitions, in principle, only occur in the thermodynamic limit of a large system, there has been interest in phase changes in small systems for many years. It is now known that particles with fewer than 100 atoms can undergo a melting transition from a solidlike phase to a liquidlike phase.^{6–16} For particles with less than 100 atoms, the properties no longer simply scale with size: the addition or subtraction of just a single atom can make a dramatic difference. For example, adding one atom to Al_{55}^+ causes the melting temperature to drop by more than 100 °C.¹⁷

How does an atomic cluster melt? Does it melt directly so that only completely solid and completely liquid clusters exist^{18–20} or are partially melted intermediates involved?^{21,22} Surface premelting, for example, has been observed in many simulations,^{23–30} but only a few examples of premelting have been identified in experiments.¹⁷ This may be because experimental studies of the melting of size-selected clusters have lagged behind theoretical studies. Most of the experimental studies of cluster melting that have been performed so far are based on measuring the heat capacity as a function of temperature. A peak in the heat capacity due to the latent heat indicates melting. Because of their small size, the melting transitions for clusters are broad, and the signature of a partially melted intermediate (a broadening or asymmetry in the heat capacity peak) may not be immediately evident from the experimental results. Poland recently described a simple procedure to investigate whether an intermediate occurs in

the melting transitions of atomic clusters.³¹ He analyzed heat capacities measured for Al_{53}^+ and Al_{79}^+ and concluded that the melting of Al_{79}^+ involved an intermediate, while only solidlike and liquidlike clusters are present for Al_{53}^+ .

In the work reported here, we continue to address melting in aluminum cluster cations. We have previously reported studies of the melting of aluminum clusters with 49–83 atoms,^{17,32} and we recently reported measurements of the heat capacities for aluminum clusters with 31, 34, 37, 39, 40, 44, and 46 atoms along with density functional theory studies aimed at investigating connections between the melting behavior of the clusters and their geometries and other related properties.³³ Here, we report heat capacity measurements for all clusters in the 16 to 48 atom size range. We use a procedure similar to that described by Poland to examine the melting transitions. For all the clusters in the 16–48 atom size regime, we find that the results can be fitted using a two-state model incorporating only solidlike and liquidlike clusters. In other words, the melting transitions apparently occur without the involvement of a partially melted intermediate. We have also reanalyzed our previously reported measurements for aluminum clusters with 49 to 83 atoms using both the two-state model and a three-state model that incorporates an intermediate between the solidlike and liquidlike clusters. In addition to providing information about the role of intermediates in the melting transitions, this analysis provides more reliable values for the melting temperatures, and the latent heats than can be obtained from a direct examination of the experimental results. So, we present here what we believe to be the most reliable values for these quantities.

Heat capacities are determined for size-selected aluminum cluster cations by measuring their dissociation thresholds as a function of temperature. The change in the dissociation threshold with temperature is proportional to the change in the internal energy with temperature, which is the heat capacity. Starting at low temperature, the dissociation threshold

decreases as the temperature is raised due to the heat capacity of the solid. At the melting transition, there is a sharp drop in the dissociation threshold due to the latent heat, and then the dissociation threshold of the liquid clusters gradually decreases due to the heat capacity of the liquid. The signature of a melting transition is the jump in the dissociation threshold, or the corresponding peak in the heat capacity, due to the latent heat.

EXPERIMENTAL METHODS

The experimental apparatus and methods have recently been described in detail.^{15,32} Only a brief overview is provided here. The cluster ions are generated by laser vaporization of a liquid metal target. The liquid metal target provides stable cluster ion signals because the liquid continuously refreshes the surface.³⁴ The clusters are carried through the source and into a temperature variable extension by a helium buffer gas flow. The temperature of the extension can be adjusted between 77 and 1100 K. Previous studies, where we adjusted the length of the extension and the size of the entrance and exit apertures, have indicated that the clusters achieve thermal equilibrium as they travel through the extension. At the end of the extension, some of the cluster ions exit through a small aperture; they are then focused into a quadrupole mass spectrometer where a specific cluster size is selected. The size-selected clusters are then focused into a collision cell containing 1 torr of helium gas. As the cluster ions enter the collision cell, they undergo many collisions with the helium gas. Each collision converts a small fraction of the ions' translational energy into internal energy and translational energy of the helium collision partner. Eventually, the translational energy of the cluster ions is thermalized, and then further collisions with the helium thermalizes the cluster's internal energy. If the initial translational energy of the ions as they enter the collision cell is high enough, some of the clusters may dissociate while they are hot. The fragments and undissociated cluster ions are then carried across the collision cell by a weak electric field. At the other side of the collision cell, some of the ions exit through a small aperture. The ions that exit are focused into a quadrupole mass spectrometer where they are mass analyzed and then detected.

EXPERIMENTAL RESULTS

The aluminum clusters dissociate by the sequential evaporation of atoms. The fraction of the cluster ions that dissociate is determined from the mass spectra, and these measurements are performed as a function of the initial translational energy of the cluster ions as they enter the collision cell. The translational energy required for 50% of the ions to dissociate (TE50%D) is determined by plotting the fraction of ions that dissociate against translational energy and by performing a linear regression. TE50%D is then determined as a function of the temperature of the extension, in 50 K intervals. The derivative of TE50%D with respect to temperature is proportional to the heat capacity. The proportionality constant is the fraction of the cluster ion's translational energy

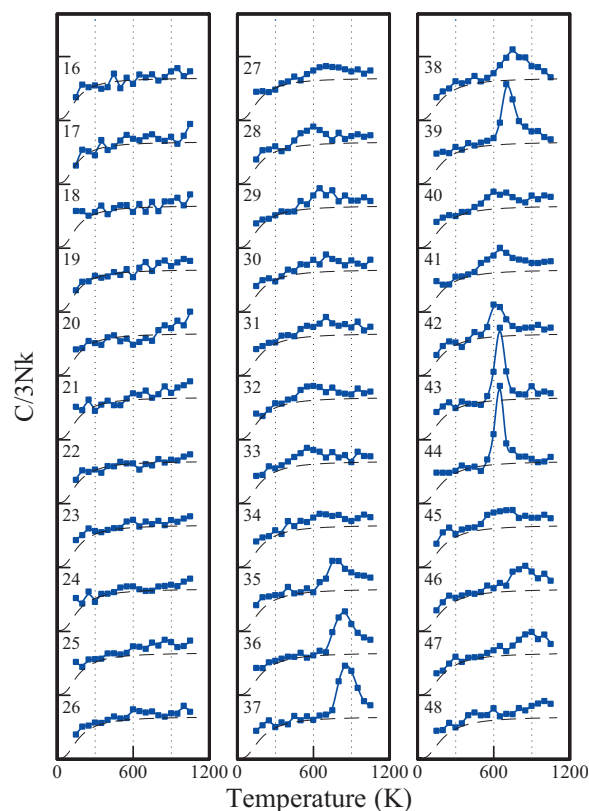


FIG. 1. (Color online) Heat capacities measured as a function of temperature for aluminum clusters with 16–48 atoms. The points are the experimental measurements, and the thick solid lines are spline fits to the measured values. The thin dashed line is the heat capacity obtained from a modified Debye model (Ref. 37). The heat capacities are given relative to the classical value of $3Nk$, where k is the Boltzmann constant and $3N$ is given by $3n-6+3/2$, where n is the number of atoms in the cluster.

that is converted into internal energy as it enters the collision cell. This is determined from a simple modified impulsive collision model.^{35,36}

Figure 1 shows a plot of the heat capacities determined for clusters with 16–48 atoms. The points are the measured values, the thick solid lines are spline fits to the measured values, and the thin dashed lines are the heat capacities calculated with a modified Debye model that accounts for the finite size of the cluster.³⁷ The measured values are given relative to the classical value of $3Nk$, where k is the Boltzmann constant and $3N$ is given by $3n-6+3/2$, where n is the number of atoms in the cluster. Some of the clusters show substantial peaks in their heat capacities. These peaks are believed to result from melting transitions. The area under the peaks is the latent heat. It is evident from Fig. 1 that there are substantial variations in both the width of the peak and the peak intensity. The smallest cluster to show a well-defined peak in its heat capacity is Al_{28}^+ , which shows a relatively broad peak centered around 600 K. Al_{27}^+ shows a small broad peak centered around 700 K. For smaller clusters, those with 26 to 16 atoms, the heat capacities are relatively flat and featureless. The measurements become more difficult with decreasing cluster size because the change in the internal energy with temperature becomes smaller. For

this reason, only a few measurements were performed for clusters with fewer than 16 atoms, and we do not report the results here except to note that a substantial peak was not found in the heat capacities for Al_{13}^+ . For some clusters in the 16 to 26 atom size range, there is a hint that the melting temperatures are above the temperature range examined here. The heat capacities for Al_{20}^+ and Al_{21}^+ , for example, both increase significantly at the upper end of the temperature range.

COMPARISON WITH THE PREDICTIONS OF A TWO-STATE MODEL

Here, we describe an approach in analyzing the peaks in the heat capacities that is similar to that recently described by Poland.³¹ If the transition between the solidlike and liquidlike clusters involves only two states, then we can treat the process as an equilibrium,



with

$$K = \frac{[L]}{[S]} = \exp\left[-\frac{\Delta G_m}{RT}\right], \quad (2)$$

where ΔG_m is the free energy change for the melting transition. If T_m is the midpoint of the transition, where $K(T_m) = 1$ and $\Delta G_m = 0$, then $\Delta S_m = \Delta H_m/T_m$ and ΔH_m are the entropy and enthalpy changes for the melting transition, respectively. So, Eq. (2) can be rewritten as

$$K(T) = \exp\left[-\frac{\Delta H_m}{R}\left(\frac{1}{T} - \frac{1}{T_m}\right)\right], \quad (3)$$

and at any temperature the fraction of liquid clusters is

$$f_L = \frac{K(T)}{1 + K(T)}. \quad (4)$$

The heat capacity of the clusters is given by

$$C = (1 - f_L)C_S + f_L C_L + \frac{d(f_L \Delta H_m)}{dT}, \quad (5)$$

where C_S and C_L are the heat capacities of the solid and liquid clusters, respectively, and the third term results from the latent heat. As a first estimate for the heat capacity of the solid clusters, we use the heat capacity derived from a modified Debye model.³⁷ It appears that the measured heat capacities are slightly (typically by 5%–10%) larger than the predicted values (see below). This difference could be real or it may indicate that the heat capacities are slightly underestimated. To correct for this discrepancy, we set

$$C_S = S_S \frac{dE_{MD}}{dT}, \quad (6)$$

where E_{MD} is the internal energy from the modified Debye model and S_S is a scale factor. The heat capacity for the liquid cluster is expected to be slightly larger than that for the solid, and this is indeed found in the experimental results

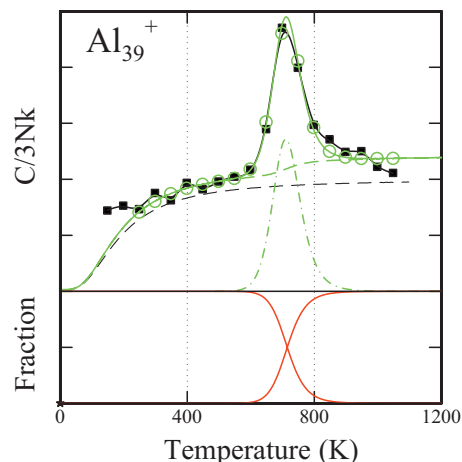


FIG. 2. (Color online) Comparison of the measured heat capacities for Al_{39}^+ to the predictions of the two-state model described in the text. The filled black points are the measured values. The solid black line running through the filled points is a spline fit. The thin dashed black line shows the heat capacity from the modified Debye model (Ref. 37). The open green (gray) points are the fit of the two-state model with $\Delta T = 50$ K. The solid green (gray) line is the prediction of the two-state model with $\Delta T = 5$ K. The dashed green (gray) line shows the heat capacity calculated from the first two terms in Eq. (8) (i.e., the heat capacity without the contribution from the latent heat). The dashed-dotted line shows the contribution from the latent heat. The lower panel shows the relative abundances of solid and liquid clusters as a function of temperature.

where the liquid clusters have heat capacities which are, on average, around 10% larger than those for the solid (see below). To account for this difference, we use

$$C_L = S_L S_S \frac{dE_{MD}}{dT}, \quad (7)$$

where S_L is the scale factor that relates the heat capacity of the liquid clusters to the solid. Thus, rewriting Eq. (5), we have

$$C = (1 - f_L) S_S \frac{\Delta E_{MD}(T)}{\Delta T} + f_L S_S S_L \frac{\Delta E_{MD}(T)}{\Delta T} + \frac{\Delta(f_L \Delta H_m)}{\Delta T}. \quad (8)$$

f_L in this equation is a function of T_m and ΔH_m . To fit Eq. (8) to the measured heat capacities, there are four unknown parameters that must be adjusted: T_m , ΔH_m , S_S , and S_L . A computer program was written to adjust these four parameters using a least squares criteria to fit the measured points. An example of a fit is shown in Fig. 2 for Al_{39}^+ . In this figure, the filled points are the measured heat capacities. The thin dashed black line shows the heat capacity derived directly from the modified Debye model.³⁷ The open circles are the heat capacities determined using a least squares fit of the two-state model described above. The fit was only performed for points with $T > 223$ K. The low temperature measurements systematically diverge from the predictions of the modified Debye model for most cluster sizes. The fit was done with a ΔT of 50 K to match the value used in the

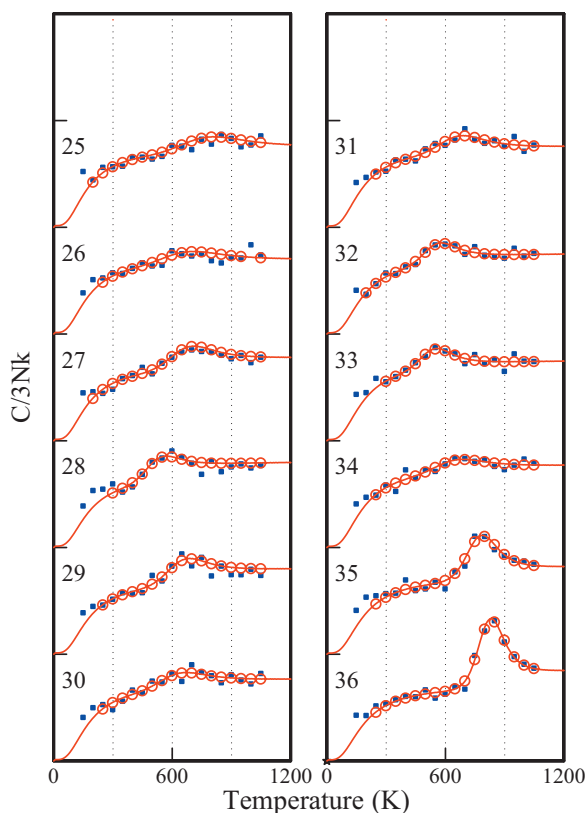


FIG. 3. (Color online) Comparison of the measured heat capacities for clusters with 25–36 atoms with the predictions of the two-state model described in the text. The solid blue (dark gray) points are the measured heat capacities, while the open red (dark gray) points are the heat capacities calculated with the two-state model with $\Delta T=50$ K. The solid red (dark gray) line shows heat capacities calculated with $\Delta T=5$ K.

experiments. The solid green (gray) line that goes through the calculated points was determined with ΔT of 5 K. There is not much difference between the points and the line, which indicates that the size of the ΔT used here does not significantly influence the results. The thicker dashed green (gray) line shows the first two terms in Eq. (8) (i.e., the heat capacity without the contribution from the latent heat). The dashed-dotted line shows the contribution from the latent heat. The lower panel in Fig. 2 shows the relative abundances of solid and liquid clusters as a function of temperature.

Figures 3 and 4 show the fits to the heat capacities for clusters with 25–48 atoms. For most clusters with $n < 25$, the heat capacities are relatively flat and featureless, and reliable fits could not be obtained. In Figs. 3 and 4, the filled points are the experimental results and the open points are fits of the two-state model with $\Delta T=50$ K. The solid lines in the figures were calculated with $\Delta T=5$ K. In the 25–48 atom size range, where good fits were obtained, some clusters have substantial peaks in their heat capacities, Al_{43}^+ and Al_{44}^+ , for example, while for other clusters the peaks are small. For clusters with 25, 26, 31, 34, and 48 atoms, the peaks are sufficiently small that the values for the melting temperatures and latent heats that are derived from the fits should be treated with some caution. For a given melting temperature,

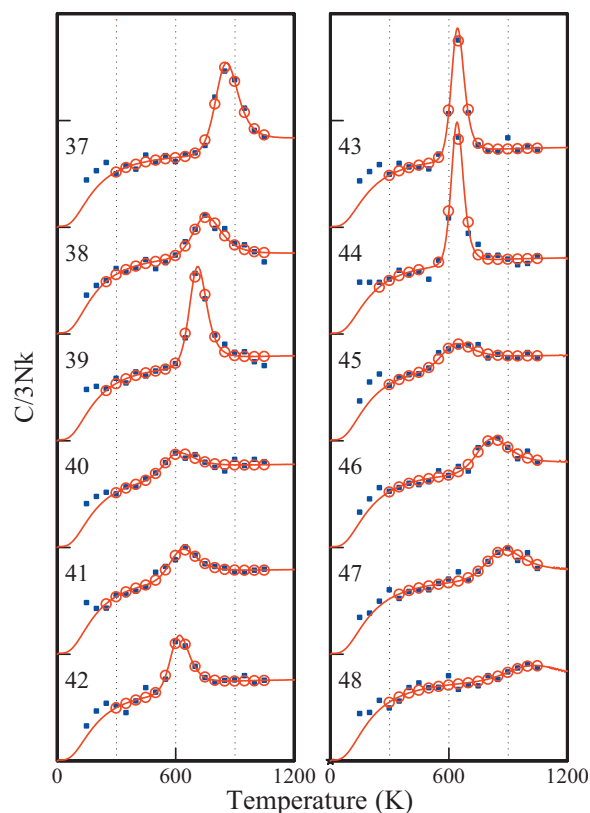


FIG. 4. (Color online) Comparison of the measured heat capacities for clusters with 37–48 atoms with the predictions of the two-state model described in the text. The solid blue (dark gray) points are the measured heat capacities, while the open red (dark gray) points are the heat capacities calculated with the two-state model with $\Delta T=50$ K. The solid red (dark gray) line shows heat capacities calculated with $\Delta T=5$ K.

the width of the transition depends on the latent heat. A large latent heat leads to a sharp well-defined peak in the heat capacity. As the latent heat becomes smaller, the peaks become broader and the peak intensity diminishes rapidly. This can be seen by comparing the results for Al_{40}^+ , Al_{41}^+ , Al_{42}^+ , and Al_{43}^+ in Fig. 4. The latent heats for these clusters, determined from the fits, are 60, 73, 99, and 161 kJ mol^{-1} respectively. The melting temperature also affects the shape of the peaks in the heat capacity. For a given latent heat, the peak in the heat capacity becomes broader as the melting temperature is raised. For example, both Al_{37}^+ and Al_{43}^+ have latent heats that are 161 kJ mol^{-1} according to the fits shown in Fig. 4. However, the peak for Al_{43}^+ is substantially narrower than that for Al_{37}^+ .

Figure 5(a) shows the melting temperatures deduced from the fits shown in Figs. 3 and 4 plotted against cluster size. Results for clusters with 49–83 atoms are also shown (see below). The dashed horizontal line in Fig. 5(a) shows the bulk melting point (934 K). There are large size-dependent fluctuations in the melting temperatures. As noted above, the values for clusters with 25, 26, 31, 34, and 48 atoms should be treated with some caution because the peaks in the heat capacities are small. According to the figure, Al_{48}^+ has a melting temperature significantly above the bulk value. From

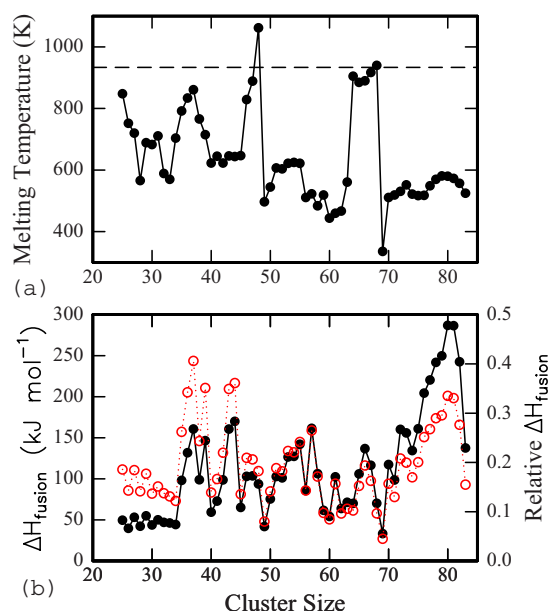


FIG. 5. (Color online) (a) The melting temperature obtained from the two-state model plotted against the cluster size. The horizontal dashed line shows the bulk melting point (934 K). (b) The latent heat per cluster (in kJ mol^{-1}) derived from the two-state model plotted against the cluster size (filled black points and left hand scale). The open red (dark gray) points show the relative latent heat plotted against the right hand scale. The relative latent heat is the latent heat determined using the two-state model divided by n times the bulk latent heat per atom (10.7 kJ mol^{-1}).

the fit shown in Fig. 4, this high melting temperature is a consequence of the rise in the heat capacity at the high temperature end of the range investigated in the experiments. This can be taken to indicate that the melting temperature lies above the bulk melting point, but the value which comes from the fit shown in Fig. 4 is probably not very reliable. As noted above, the heat capacities for some of the smaller clusters, Al_{20}^+ and Al_{21}^+ in particular, increase significantly at the upper end of the temperature range. It is likely that these clusters also have melting temperatures that lie above the bulk melting point. Clusters with melting temperatures above the bulk melting point have been found before. Both tin³⁸ and gallium¹⁵ clusters have melting temperatures which lie above their respective bulk melting points. However, in these examples all of the small clusters have melting points that lie above the bulk, and the size regime where the clusters drop below the bulk value is not known. Clusters are expected to have melting temperatures below the bulk melting temperature. The melting points of small particles are known to initially decrease with particle size because of the increase in the surface to volume ratio.¹⁻⁵ The elevated melting temperatures found for tin and gallium clusters have been attributed to the clusters having different structures and bondings compared to those of the bulk material.^{29,39-41}

The lower half of Fig. 5 shows the latent heats (obtained from the fits of the two-state model) plotted against the cluster size. The filled points show the latent heat per cluster in kJ mol^{-1} (left hand scale). The open points show the relative latent heat plotted against the right hand scale. The relative

latent heat is the measured latent heat divided by n times the bulk latent heat per atom (10.7 kJ mol^{-1}). The latent heats are relatively small, varying between 10% and 40% of the bulk value. There are substantial size-dependent variations in the latent heats.

INTERMEDIATES IN THE MELTING OF CLUSTERS WITH 49–83 ATOMS

In all cases shown in Figs. 3 and 4 (clusters with 25–48 atoms), the shape of the peak in the heat capacity can be reasonably well fitted using the simple two-state model to describe the melting transition. Thus, these clusters apparently melt without the involvement of partially melted intermediates: the transition from solidlike to liquidlike occurs in a single step. However, previous work has indicated that this is not true for some slightly larger clusters. The heat capacity peaks for Al_{51}^+ and Al_{52}^+ , for example, appear broadened and asymmetric.¹⁷ Thus, we have attempted to fit the two-state model described above to the heat capacity plots for the larger clusters for which measurements have been performed (49–83 atoms). Representative results are shown in Fig. 6. In the left hand panel, we show results for clusters with 50–53 atoms. The results for Al_{50}^+ are well fitted by the two-state model. Clusters with 51 and 52 atoms were previously been identified as having asymmetric peaks. In the case of Al_{51}^+ , the least squares fitting procedure used to fit the two-state model to the measured values adjusts the scale factor for the heat capacity of the solid clusters (S_S) to minimize the effect of the asymmetry. This also occurs for Al_{52}^+ , but the fitting procedure is less successful in this case because the heat capacity peak is more asymmetric. For Al_{53}^+ the two-state model provides a good fit to the measured heat capacities. This is also true for Al_{55}^+ in Fig. 6. The situation for Al_{56}^+ is complicated by a dip in the heat capacities at around 400 K. This dip, which occurs for a number of clusters in this size regime, is believed to result from annealing transitions.¹⁷ At low temperature, the clusters are trapped in one or more high energy conformations. However, as the temperature is raised, the metastable conformations convert into the ground state. This causes a jump in the cluster's dissociation threshold, which leads to the dip in the heat capacities.³² Since the dip is not incorporated into the two-state model we remove the point causing the dip from the fitting procedure. As can be seen from Fig. 6, the heat capacity peak for Al_{56}^+ is significantly broader than the prediction of the two-state model.

In addition to clusters with 51, 52, and 56 atoms, we found two more clear-cut examples where melting involves an intermediate: Al_{61}^+ and Al_{83}^+ . The results of the two-state model for Al_{83}^+ are shown in the right hand panel in Fig. 6. For both Al_{61}^+ and Al_{83}^+ the two-state model fails to account for a high temperature shoulder on the heat capacity peak. In all other cases, the heat capacity peaks for clusters in the 49–83 atom size range could be fitted using the two-state model. In this regard, we differ from the conclusion reached by Poland, who indicated that the heat capacity peak for Al_{79}^+ could not be fitted with a two-state model. This difference results because we take into account the finite resolution of the measurements. An expanded view of the results

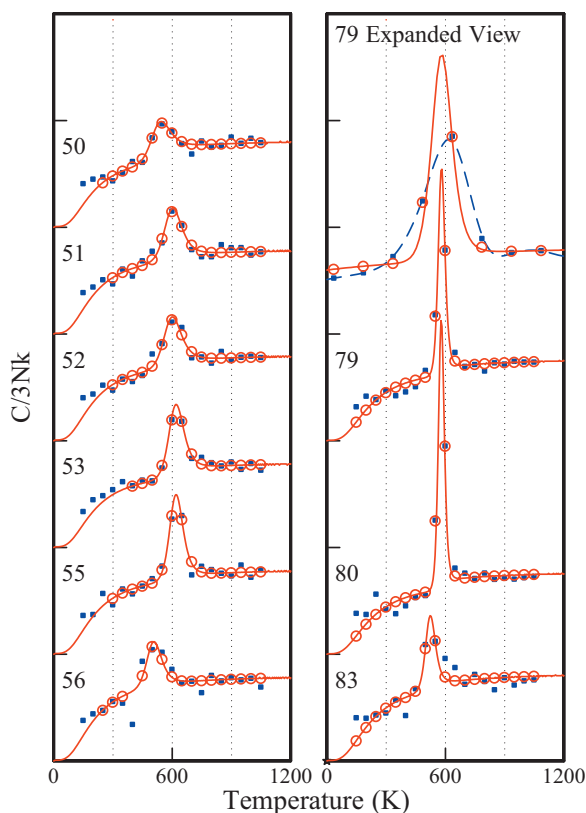


FIG. 6. (Color online) Comparison of the measured heat capacities for clusters with 50–53, 55, 56, 79, 80, and 83 atoms with the predictions of the two-state model described in the text. The solid blue (dark gray) points are the measured heat capacities, while the open red (dark gray) points are the heat capacities calculated with the two-state model with $\Delta T=50$ K. The solid red (dark gray) line shows heat capacities calculated with $\Delta T=5$ K. An expanded view of the heat capacity peak for Al_{79}^+ (where the temperature scale is multiplied by 3) is shown at the top of the right hand panel. The dashed blue (dark gray) line in the expanded view is a spline fit to the measured heat capacity points. This probably overestimates the width of the transition and makes it appear asymmetric.

for Al_{79}^+ (where the temperature scale is multiplied by 3) is shown in the right hand panel of Fig. 6. The two-state model calculated with $\Delta T=50$ K (the open circles) is a good fit to the measured values (the filled points). The solid line shows the heat capacity calculated with the two-state model with $\Delta T=5$ K. This shows what the peak would look like if it were measured with a higher resolution. The dashed line shows a spline fit to the measured heat capacities that we showed in the original report of these results.³² This overestimates the width of the transition and makes it appear asymmetric. The spline fit is similar to the interpolation used by Poland to extract average internal energies from the heat capacities. The overestimation of the width of the transition in the interpolation leads to the conclusion that the results for Al_{79}^+ could not be fitted by a two-state model. The problem of the transition being significantly narrower than the interpolation is limited to clusters where the latent heat is large (a large latent heat leads to a narrow transition within the framework of the two-state model). This problem is most significant for clusters with 76–82 atoms. As is apparent

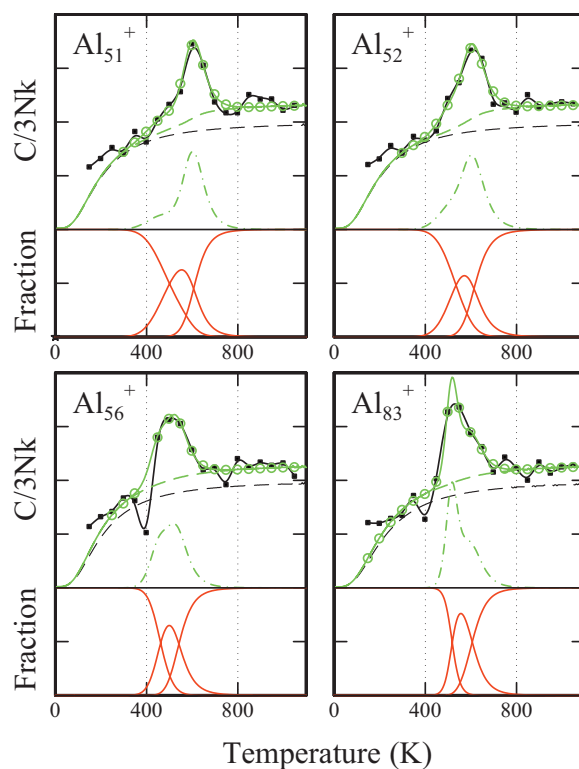


FIG. 7. (Color online) Comparison of the measured heat capacities for clusters with 51, 52, 56, and 83 atoms to the predictions of the three-state model described in the text. The filled black points are the measured values. The solid black line running through the filled points is a spline fit. The thin dashed black line shows the heat capacity from the modified Debye model (Ref. 37). The open green (gray) points are the fit of the three-state model with $\Delta T=50$ K. The solid green (gray) line is the prediction of the three-state model with $\Delta T=5$ K. The dashed green (gray) line shows the heat capacity without the contribution from the latent heat. The dashed-dotted line shows the contribution of the latent heat. The lower panel shows the relative abundances of solid, intermediate, and liquid clusters as a function of temperature.

from Fig. 5(b), these clusters are the ones with the largest latent heats.

Figure 7 shows a comparison of the experimental results for clusters with 51, 52, 56, and 83 atoms to a three-state model where melting occurs through an intermediate state,



The rest of the model follows the development of the two-state model described above. A least squares fitting procedure has six unknowns: the transition temperatures and enthalpy changes for the two transitions and the scale factors for the heat capacities of the liquid and solid phases (the scale factor for the intermediate is assumed to be given by $S_S S_L / 2$). The filled black points in Fig. 7 are the measured values. The open points are the fit of the three-state model with $\Delta T=50$ K. The solid green (gray) line is the prediction of the three-state model with $\Delta T=5$ K. The dashed green (gray) line shows the heat capacity without the contribution from the latent heat, and the dashed-dotted line shows the

TABLE I. Summary of the transition temperatures and latent heats derived from the three-state model for clusters with 51, 52, 56, 61, and 83 atoms.

Cluster	First transition temperature (K)	First latent heat (kJ mol ⁻¹)	Second transition temperature (K)	Second latent heat (kJ mol ⁻¹)
Al ₅₁ ⁺	501	36	606	96
Al ₅₂ ⁺	535	51	614	90
Al ₅₆ ⁺	462	61	542	76
Al ₆₁ ⁺	457	99	577	51
Al ₈₃ ⁺	518	128	606	97

contribution from the latent heat. The lower panel shows the relative abundances of solid, intermediate, and liquid clusters as a function of temperature. The transition temperatures and latent heats for both transitions are summarized in Table I. For Al₅₁⁺ and Al₅₂⁺, the first transition has a lower latent heat than the second, and so the peak in the heat capacity is characterized by a shoulder at a lower temperature compared to the main peak. The melting transitions for Al₆₁⁺ and Al₈₃⁺ show the reverse behavior with a shoulder at a higher temperature compared to the main peak. For Al₅₆⁺, the latent heat for the first transition is slightly smaller than for the second.

We return now to reconsider the size-dependent variations in the melting temperatures shown in Fig. 5. Beyond Al₄₈⁺, the melting temperature drops precipitously from above the bulk melting point to around 500 K. The melting temperature for clusters with around 50–60 atoms then fluctuates between 450 and 650 K. Beyond Al₆₃⁺, the melting temperature suddenly jumps up to be close to the bulk value. The melting point remains high for five clusters then drops precipitously. For several clusters in the 60–70 atom size range, the latent heats are small and the peaks in the heat capacities are small and broad. We show in Fig. 8 the fits of the two-state model to the measured heat capacities for clusters with 60–71 atoms. For clusters with 64, 68, and 69 atoms, the heat capacity peaks are sufficiently broad that we would be hard pressed to identify the melting temperature without the model. These clusters are all in the transition regions where the melting temperature is changing rapidly. According to the fit, Al₆₄⁺ has a melting temperature that is similar to Al₆₅⁺ and Al₆₈⁺ has a melting temperature that is similar to Al₆₇⁺. On the other hand, Al₆₉⁺ has a melting temperature that is significantly lower than that of Al₇₀⁺. Al₆₉⁺, with a melting temperature of 336 K, is the aluminum cluster with the lowest melting temperature. The melting temperature for Al₆₉⁺ is low enough that melting occurs where the heat capacity predicted by the modified Debye model starts to decrease rapidly. For this reason, the melting transition for Al₆₉⁺ is indicated by an inflection rather than by a peak.

DISCUSSION

The melting temperatures for aluminum cluster cations in the size range examined here undergo large size-dependent fluctuations. In several cases, adding or subtracting a single

atom causes the melting temperature to change by more than 300 °C. The substantial fluctuations in the melting temperatures found in the recent experimental studies for sodium, gallium, and aluminum clusters have provided the motivation for a number of theoretical studies directed at uncovering the cause of the fluctuations.^{41–49} Aguado and Lopez pointed to a correlation between the compactness (in particular, a short distance between the surface atoms and the core atoms) and a high melting temperature in sodium clusters.⁴⁷ Recent calculations indicate that a similar correlation may also exist for aluminum clusters.³³

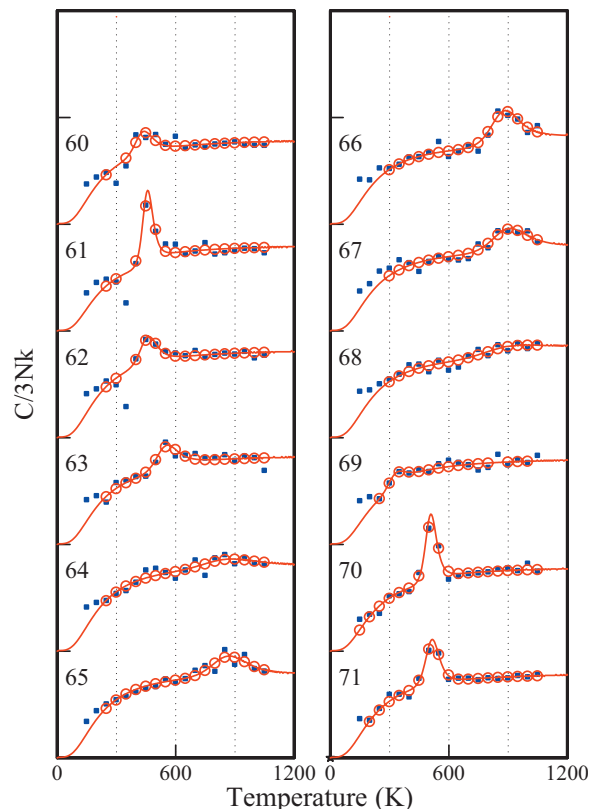


FIG. 8. (Color online) Comparison of the measured heat capacities for clusters with 60–71 atoms with the predictions of the two-state model described in the text. The solid blue (dark gray) points are the measured heat capacities, while the open red (dark gray) points are the heat capacities calculated with the two-state model with $\Delta T=50$ K. The solid red (dark gray) line shows heat capacities calculated with $\Delta T=5$ K.

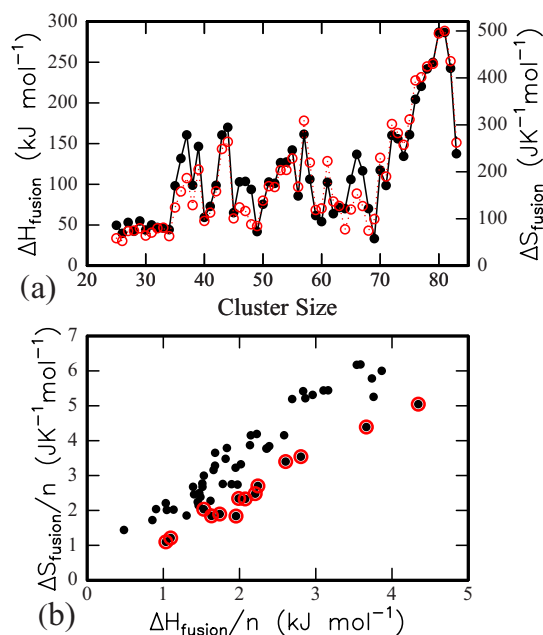


FIG. 9. (Color online) (a) Comparison of the latent heats with the entropies of melting for aluminum clusters with 25–83 atoms. The filled black points are the latent heats and the open red (dark gray) points are the entropies. (b) Entropy of melting per atom plotted against the latent heat per atom for aluminum clusters with 25–83 atoms. The points that are circled in red (dark gray) are due to clusters with melting temperatures greater than 750 K.

There appear to be three regions of high melting temperature: around 37, 47, and 66 atoms. The high melting temperatures around 37 atoms appear to be correlated with a maximum in the latent heats (see Fig. 5). However, another maximum in the latent heats at around 43 and 44 atoms is not correlated with elevated melting temperatures. The high melting temperatures at around 47 atoms and 66 atoms are also not correlated with elevated latent heats. The lack of a correlation between the latent heats and the melting temperatures occurs because the melting temperature depends on both the latent heat and the entropy of melting. An estimate of the entropy of melting can be obtained from $\Delta S_m = \Delta H_m/T_m$. The entropy of melting determined in this way is plotted in Fig. 9(a) along with the latent heats. The entropies of melting (open points) and the latent heats (filled points) are correlated. This correlation has been seen before in the melting of sodium⁵⁰ and gallium¹⁶ clusters, and so it appears to be quite general. Williams *et al.* previously commented on a correlation between the entropy and enthalpy of melting for a series of hydrocarbons.⁵¹ They attributed this relationship to the decrease in intermolecular bonding on melting being correlated with an increase in intramolecular motion in the liquid. Figure 9(b) shows a plot of the entropy of melting per atom against the latent heat per atom for the aluminum clusters. This figure provides a better indication of the degree of correlation between these two quantities than Fig. 9(a).

The origin of the entropy-enthalpy compensation for cluster melting transitions may simply be that clusters with large latent heats generally have more strongly bound solidlike states, and so they are stiffer and have higher average vibra-

tional frequencies. For these clusters, the solid form has a lower entropy, and hence the entropy change on going to the liquid is larger. Note in Fig. 9(b) that a range of ΔS_m values is associated with each value of ΔH_m . We have identified in Fig. 9(b) the clusters that have high melting temperatures (i.e., greater than 750 K) by red (dark gray) circles around the points. The high melting temperature clusters are found for a wide range of ΔH_m values. However, for a given value of ΔH_m , a high melting temperature is always associated with a low value of ΔS_m . A small entropy change occurs when the solidlike cluster is less stiff than average and has lower than average vibrational frequencies.

Except for a few clusters (51, 52, 56, 61, and 83), the width of the peaks in the heat capacities can be fitted by the two-state model. Within the framework of this model, the width of the transition depends on the size of the latent heat and, to a lesser extent, on the melting temperature. The width increases as the latent heat decreases and as the melting temperature increases. In previous work, the wide variation in the width of the peak in the heat capacity has been attributed to structural effects rather than to thermodynamic effects. Gallium clusters also show a wide variation in the size and width of their heat capacity peaks.^{15,16} The melting of Ga_{30} and Ga_{31} has been investigated by Joshi *et al.* using molecular dynamics simulations with density functional theory.⁴⁴ In the experiments, Ga_{31}^+ melts with a relatively sharp peak in its heat capacity, while Ga_{30}^+ lacks a well-defined peak. In the calculations, it was found that Ga_{31} has an “ordered” ground state in the sense that most of the atoms experience a similar bonding environment with similar bond lengths and bond strengths, while Ga_{30} has a “disordered” ground state. It was suggested that a large group of atoms bound together with similar strengths will melt together while a disordered cluster is expected to show a broad continuous phase transformation. A similar argument has been put forward to explain the widths of the transitions found for aluminum clusters.³³ In this case, Al_{34}^+ was selected as an example of a cluster which shows a broad melting transition, while Al_{44}^+ was chosen to illustrate a cluster with a sharp peak in its heat capacity. In the calculations, Al_{34} had a disordered ground state, while the ground state of Al_{44} was ordered. As can be seen from Figs. 3 and 4, the melting transitions for both clusters can be fitted by the two-state model. The melting transition for Al_{34}^+ is broad because the latent heat is small. It is not necessary to invoke the idea that melting occurs gradually to explain the width of the transition. Indeed, an agreement with the two-state model suggests that the transition is direct (i.e., it does not involve partially melted intermediates). On the other hand, a cluster with a disordered ground state, such as Al_{34}^+ , is expected to melt with a small latent heat. So, a correlation between disordered ground states and broad melting transitions is expected. A cluster with a disordered ground state is also expected to have a small entropy change for melting, and this may also contribute to correlation between the latent heat and the entropy of melting.

Using the least squares criteria to fit the two-state model to the measured heat capacities does not provide a particularly discriminating approach in identifying cases where melting involves an intermediate. The results for Al_{51}^+ illus-

trate this point. A reasonable fit to the experimental results could be obtained with the two-state model, even though the peak in the heat capacity appears asymmetric and the three-state model clearly provides a better fit (see Fig. 7). In cases where the three-state model provides a much better fit to the measured heat capacities (51, 52, 56, 61, and 83), latent heats are determined for the two transitions (solid to intermediate and intermediate to liquid). From Table I, it can be seen that for Al_{51}^+ and Al_{52}^+ the latent heat for the first transition is significantly less than that for the second. On the other hand, for Al_{61}^+ and Al_{83}^+ , the latent heat for the first transition is significantly more than that for the second. For Al_{56}^+ , the latent heats for the two transitions are roughly the same.

The three-state model provides no insight into the nature of the intermediate states. Perhaps the most plausible explanation is that the intermediate results from surface premelting, where the surface layer of the cluster melts before the core. Surface premelting is usually associated with a small premelting peak that precedes the main melting peak. However, examples where the premelting peak is stronger than the actual melting peak have been observed in simulations for larger sodium clusters,³⁰ where this situation was given the name “postmelting.” These results represent the first experimental observation of this phenomenon.

Another possible explanation for the two peaks in the heat capacity near the melting transition is that they come from a structural transition. For example, Doye and Wales showed that the lowest energy structure for a 37-atom Lennard-Jones cluster is fcc, but an icosahedral structure is slightly higher in energy and becomes entropically preferred as the temperature is raised.⁵² A transition between the fcc structure and the icosahedral structure occurs through sampling the liquid phase (i.e., the transition is fcc → liquid → icosahedral). This structural transition leads to a small peak in the heat capacity before the main melting transition. Cleveland *et al.* reported that in simulations of large gold clusters (Au_{146} and Au_{459}) melting occurs through an icosahedral intermediate or precursor.⁵³ Thus, structural transitions that precede the melting transition are a plausible alternative explanation for the melting transitions that occur through an intermediate. However, it is difficult to imagine that this process can lead to a situation where the latent heat for the first transition is larger than that for the second. So, this postmelting behavior must be due to partially melted (perhaps surface-melted) intermediates.

CONCLUSIONS

In this paper, we have reported heat capacity measurements for aluminum clusters in the 16–48 atom size range. The results for these clusters and the previously reported results for clusters with 49–83 atoms have been compared to the predictions of a two-state melting model and, where appropriate, a three-state model. For most clusters with 25–83 atoms, the results can be adequately fitted by the two-state model. In particular, variations in the widths of the melting transitions can be accounted for by the two-state model. The peaks in the heat capacity become broader as the latent heat decreases and the melting temperature increases. For clusters with 51, 52, 56, 61, and 83 atoms, the results cannot be adequately fitted by the two-state model, which indicates that melting involves an intermediate. Both premelting transitions (where the latent heat for the first transition is smaller than that for the main melting transition) and postmelting transitions (where the latent heat for the second transition is smaller than that for the first) were found. The most likely explanation for both the premelting and postmelting transitions is that they arise from an intermediate with a partially melted or fully melted surface. The premelting transition may also be due to a structural transformation where the liquid state is involved in the interconversion.

There are wide variations in both the melting temperatures and the latent heats. There are three regions of high melting temperatures: around 37, 47, and 66. The variations in the latent heats and melting temperatures are not correlated. However, the latent heats are correlated with the entropies of melting. This correlation probably results from clusters with larger latent heats that are more strongly bound and hence stiffer with higher average vibrational frequencies. Thus, the solidlike clusters have low entropies, and the entropy change on melting is larger. Theoretical studies suggest that clusters with low latent heats are more disordered, and this may also contribute to the correlation. The high melting temperatures observed for some clusters are not associated with high latent heats. However, for a particular latent heat, the high melting temperature clusters are the ones with the lowest entropy changes.

ACKNOWLEDGMENT

We are grateful for the support of the National Science Foundation.

¹M. Takagi, J. Phys. Soc. Jpn. **9**, 359 (1954).

²Ph. Buffat and J. P. Borell, Phys. Rev. A **13**, 2287 (1976).

³P. R. Couchman and W. A. Jesser, Nature (London) **269**, 481 (1977).

⁴S. L. Lai, J. Y. Guo, V. Petrova, G. Ramanath, and L. H. Allen, Phys. Rev. Lett. **77**, 99 (1996).

⁵P. Pawlow, Z. Phys. Chem., Stoichiom. Verwandtschaftsl. **65**, 545 (1909).

⁶C. L. Briant and J. J. Burton, J. Chem. Phys. **63**, 2045 (1975).

⁷R. S. Berry, J. Jellinek, and G. Natanson, Chem. Phys. Lett. **107**, 227 (1984).

⁸P. Labastie and R. L. Whetten, Phys. Rev. Lett. **65**, 1567 (1990).

⁹D. J. Wales and R. S. Berry, J. Chem. Phys. **92**, 4473 (1990).

¹⁰D. J. Wales and R. S. Berry, Phys. Rev. Lett. **73**, 2875 (1994).

¹¹R. E. Kunz and R. S. Berry, Phys. Rev. E **49**, 1895 (1994).

¹²M. Schmidt, R. Kusche, W. Kronmüller, B. von Issendorff, and H. Haberland, Phys. Rev. Lett. **79**, 99 (1997).

¹³M. Schmidt, R. Kusche, B. von Issendorff, and H. Haberland,

- Nature (London) **393**, 238 (1998).
- ¹⁴M. Schmidt and H. Haberland, *C. R. Phys.* **3**, 327 (2002).
- ¹⁵G. A. Breaux, R. C. Benirschke, T. Sugai, B. S. Kinnear, and M. F. Jarrold, *Phys. Rev. Lett.* **91**, 215508 (2003).
- ¹⁶G. A. Breaux, D. A. Hillman, C. M. Neal, R. C. Benirschke, and M. F. Jarrold, *J. Am. Chem. Soc.* **126**, 8628 (2004).
- ¹⁷G. A. Breaux, C. M. Neal, B. Cao, and M. F. Jarrold, *Phys. Rev. Lett.* **94**, 173401 (2005).
- ¹⁸J. P. Rose and R. S. Berry, *J. Chem. Phys.* **98**, 3246 (1993).
- ¹⁹J. P. Rose and R. S. Berry, *J. Chem. Phys.* **98**, 3262 (1983).
- ²⁰B. Vekhter and R. S. Berry, *J. Chem. Phys.* **106**, 6456 (1997).
- ²¹R. E. Kunz and R. S. Berry, *Phys. Rev. Lett.* **71**, 3987 (1993).
- ²²R. E. Kunz and R. S. Berry, *Phys. Rev. E* **49**, 1895 (1994).
- ²³V. V. Nauchitel and A. J. Pertsin, *Mol. Phys.* **40**, 1341 (1980).
- ²⁴H.-P. Cheng and R. S. Berry, *Phys. Rev. A* **45**, 7969 (1992).
- ²⁵A. Aguado, J. M. Lopez, J. A. Alonso, and M. J. Stott, *J. Chem. Phys.* **111**, 6026 (1999).
- ²⁶F. Calvo and F. Spiegelmann, *J. Chem. Phys.* **112**, 2888 (2000).
- ²⁷Y. J. Lee, E.-K. Lee, S. Kim, and R. M. Nieminen, *Phys. Rev. Lett.* **86**, 999 (2001).
- ²⁸A. Aguado, L. M. Molina, J. M. Loez, and J. A. Alonso, *Eur. Phys. J. D* **15**, 221 (2001).
- ²⁹K. Joshi, D. G. Kanhere, and S. A. Blundell, *Phys. Rev. B* **67**, 235413 (2003).
- ³⁰F. Calvo and F. Spiegelmann, *J. Chem. Phys.* **120**, 9684 (2004).
- ³¹D. Poland, *J. Chem. Phys.* **126**, 054507 (2007).
- ³²C. M. Neal, A. K. Starace, and M. F. Jarrold, *J. Am. Soc. Mass Spectrom.* **18**, 74 (2007).
- ³³C. M. Neal, A. K. Starace, M. F. Jarrold, K. Joshi, S. Krishnamurthy, and D. G. Kanhere, *J. Phys. Chem.* (to be published).
- ³⁴C. M. Neal, G. A. Breaux, B. Cao, A. K. Starace, and M. F. Jarrold, *Rev. Sci. Instrum.* **78**, 075108 (2007).
- ³⁵M. F. Jarrold and E. C. Honea, *J. Phys. Chem.* **95**, 9181 (1991).
- ³⁶M. F. Jarrold, *J. Phys. Chem.* **99**, 11 (1995).
- ³⁷J. Bohr, *Int. J. Quantum Chem.* **84**, 249 (2001).
- ³⁸A. A. Shvartsburg and M. F. Jarrold, *Phys. Rev. Lett.* **85**, 2530 (2000).
- ³⁹Z. Y. Lu, C. Z. Wang, and K. M. Ho, *Phys. Rev. B* **61**, 2329 (2000).
- ⁴⁰K. Joshi, D. G. Kanhere, and S. A. Blundell, *Phys. Rev. B* **66**, 155329 (2002).
- ⁴¹S. Chacko, K. Joshi, and D. G. Kanhere, *Phys. Rev. Lett.* **92**, 135506 (2004).
- ⁴²K. Manninen, A. Rytkonen, and M. Manninen, *Eur. Phys. J. D* **29**, 39 (2004).
- ⁴³S. Krishnamurthy, S. Chacko, D. G. Kanhere, G. A. Breaux, C. M. Neal, and M. F. Jarrold, *Phys. Rev. B* **73**, 045406 (2006).
- ⁴⁴K. Joshi, S. Krishnamurthy, and D. G. Kanhere, *Phys. Rev. Lett.* **96**, 135703 (2006).
- ⁴⁵E. G. Noya, J. P. K. Doye, and F. Calvo, *Phys. Rev. B* **73**, 125407 (2006).
- ⁴⁶W. Zhang, F. Zhang, and Z. Zhu, *Phys. Rev. B* **74**, 033412 (2006).
- ⁴⁷A. Aguado and J. M. Lopez, *Phys. Rev. Lett.* **94**, 233401 (2005).
- ⁴⁸A. Aguado and J. M. Lopez, *J. Phys. Chem. B* **110**, 14020 (2006).
- ⁴⁹A. Aguado and J. M. Lopez, *Phys. Rev. B* **74**, 115403 (2006).
- ⁵⁰M. Schmidt, J. Donges, Th. Hippler, and H. Haberland, *Phys. Rev. Lett.* **90**, 103401 (2003).
- ⁵¹D. H. Williams, D. P. O'Brien, and B. Bardsley, *J. Am. Chem. Soc.* **123**, 737 (2001).
- ⁵²J. P. K. Doye and D. J. Wales, *Phys. Rev. Lett.* **80**, 1357 (1998).
- ⁵³C. L. Cleveland, W. D. Luedtke, and U. Landman, *Phys. Rev. Lett.* **81**, 2036 (1998).